JACS
JOURNAL OF THE AMERICAN CHEMICAL SOCIETY
Article
pubs.acs.org/JACS

Self-Decoupled Porphyrin with a Tripodal Anchor for Molecular-Scale Electroluminescence

San-E Zhu,[†,‡] Yan-Min Kuang,[†] Feng Geng,[†] Jia-Zhe Zhu,[†] Cong-Zhou Wang,[†,‡] Yun-Jie Yu,[†] Yang Luo,[†] Yang Xiao,[†,‡] Kai-Qing Liu,[†,‡] Qiu-Shi Meng,[†] Li Zhang,[†] Song Jiang,[†] Yang Zhang,[†] Guan-Wu Wang,*[,†,‡] Zhen-Chao Dong,*[,†] and J. G. Hou[†]

[†]Hefei National Laboratory for Physical Sciences at the Microscale and [‡]CAS Key Laboratory of Soft Matter Chemistry and Department of Chemistry, University of Science and Technology of China, Hefei, Anhui 230026, China

Supporting Information

ABSTRACT: A self-decoupled porphyrin with a tripodal anchor has been synthesized and deposited on Au(111) using different wet-chemistry methods. Nanoscale electroluminescence from single porphyrin molecules or aggregates on Au(111) has been realized by tunneling electron excitation. The molecular origin of the luminescence is established by the vibrationally resolved fluorescence spectra observed. The rigid tripodal anchor not only acts as a decoupling spacer but also controls the orientation of the molecule. Intense molecular electroluminescence can be obtained from the emission enhancement provided by a good coupling between the molecular transition dipole and the axial nanocavity plasmon. The unipolar performance of the electroluminescence from the designed tripodal molecule suggests that the porphyrin molecule is likely to be excited by the injection of hot electrons, and then the excited state decays radiatively through Franck–Condon $\pi^*-\pi$ transitions. These results open up a new route to generating electrically driven nanoscale light sources.

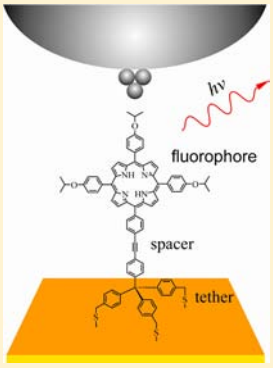

INTRODUCTION

The highly localized tunneling current in a scanning tunneling microscope (STM) can be used as a source of low-energy electrons to locally excite photon emission from metals, semiconductors, and organic molecules.[1] In recent years, STM-induced luminescence (STML) from organic molecules on metals has gained much attention for its capability in helping to develop nanoscale molecular optoelectronics and plasmonics. However, when molecules are directly adsorbed on or very close to metal surfaces, the intrinsic molecular fluorescence will be quenched by the strong interaction between the molecules and the substrate.[2−9] Decoupling the molecule from the substrate underneath is essential to the generation of molecule-specific electroluminescence near metals. To date, such decoupling has usually been realized by inserting an additional spacer layer such as an oxide, halide, or molecular multilayer in between.[2−5,10,11] The idea of chemically decoupling the emitter from the metal substrate has been proposed using a double-decker molecule by Berndt et al.[12,13] The molecule thus decoupled is found to modify the plasmonic emission profile dramatically. Nevertheless, the plasmonic nature in the observed emission suggests that the decoupling strength may still not be sufficient to generate intrinsic molecular fluorescence. Sufficient electronic decoupling and favorable axial dipole orientations are both believed to be important factors in the generation of molecule-specific fluorescence.[8,10,11,14,15] In this work, we explore the chemical approach to achieving molecule-specific emission by building the spacer and emitter together within a single molecule with controlled orientations. We shall describe the design strategy of a self-decoupled porphyrin molecule (abbreviated as **1**) bearing a rigid tripodal anchor. The challenges of its synthesis, deposition on metals, and clear characterization by STML will be addressed. Interestingly, different wet-chemistry deposition methods have been found to affect the adsorption configuration of molecules on the metal surface and resultant electroluminescent properties. A new understanding of the excitation mechanism of molecular electroluminescence in the STM junction will also be discussed briefly.

RESULTS AND DISCUSSION

Figure 1 illustrates schematically the design principle for the self-decoupled porphyrin molecule (**1**) on Au(111). The porphyrin moiety is selected as the emitter because it has proven effective in producing molecular electroluminescence in the STM junction.[10] The rigid tripodal anchor is composed of a stiff sp^3-hybridized carbon tetrahedral framework and is designed not only to bind the molecule on the Au surface through the formation of three robust Au–S bonds but also to serve as the decoupling spacer together with the linking unit of an ethynyl group. The latter is again connected to the peripheral phenyl ring of the porphyrin (Scheme 1). In this way, the porphyrin core plane will be oriented along the tip axis once the molecule stands up as designed and will thus allow for optimal coupling between the molecular transition dipole[16] and

Received: May 14, 2013
Published: September 25, 2013

   dx.doi.org/10.1021/ja4048569 | J. Am. Chem. Soc. 2013, 135, 15794−15800

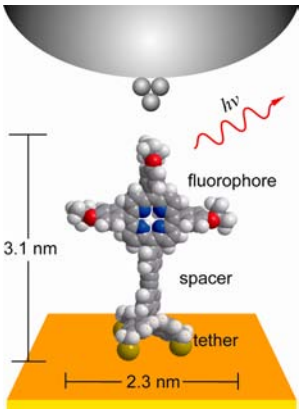

Figure 1. Schematic configuration of **1** on Au(111) and localized electrical excitation from a nanotip.

Scheme 1. Synthesis of Target Molecule 1[a]

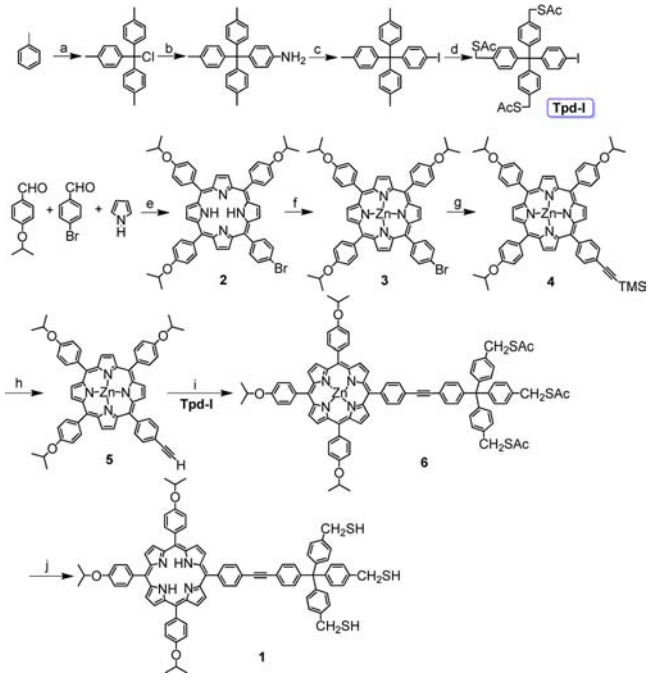

[a](a) $AlCl_3$, CCl_4, 0 °C, 1 h, rt, 2 h; AcCl, 80 °C, 2 h, 25%. (b) aniline, N_2, 200 °C, 6 h, 87%. (c) $NaNO_2$, HCl(aq) (6.1 M solution), EtOH, 0 °C, 1 h; KI, 0 °C, 1 h, rt, 19 h, 54%. (d) NBS, BPO, CCl_4, Ar, 90 °C, 3 days; KSAc, THF, reflux, 24 h, 39%. (e) EtCOOH, $(EtCO)_2O$, Ar, 170 °C, 3 h, 6%. (f) $Zn(OAc)_2{\cdot}2H_2O$, $CHCl_3$–MeOH (3/1), Ar, 80 °C, 5 h, 93%. (g) TMSA, $PdCl_2(PPh_3)_2$, PPh_3, CuI, THF, TEA, Ar, 80 °C, 48 h, 70%. (h) TBAF, THF, rt, 1 h, 82%. (i) $Pd_2(dba)_3$, PPh_3, toluene, TEA, Ar, 30 °C, 7 days, 63%. (j) conc. H_2SO_4, CH_2Cl_2, MeOH, 0 °C, 2 h, 60 °C, 12 h, 84%.

the axial nanocavity plasmon (NCP), which is expected to provide maximal emission enhancement.[8,10,11,14,15] The optimized structure of **1** has a height of ∼3.1 nm and a width of ∼2.3 nm as well as a spacer length of ∼1.5 nm.

However, the multifunctionalized complexity and the relatively large size of target molecule **1** make the sample preparation a nontrivial task, which includes both the synthesis of high-purity materials in high yield and the deposition of molecules on the metal surface with well-defined structures for STM studies. The synthesis procedure for **1** is shown in Scheme 1. The iodo-substituted tripodal rigid anchor (**Tpd-I**) was synthesized by starting from commercially available toluene and carbon tetrachloride, in reference to protocols reported in the literature.[17−23] The synthesis and isolation of the unsymmetrical porphyrin in high yield often encounter difficulties and require careful consideration in tuning the molecular solubility and polarity. 4-Isopropoxybenzaldehyde was selected to improve the solubilities and to discriminate the polarities among the porphyryin mixtures so that efficient isolation can be achieved. The condensation of pyrrole with 4-isopropoxybenzaldehyde and 4-bromobenzaldehyde in a molar ratio of 5:4:1 using the Alder−Longo method[24] gave porphyrin **2** in 6% yield. **2** was then metallized by zinc acetate dihydrate to yield zinc porphyrin **3** in a yield of 93%. Sonogashira coupling of **3** with trimethylsilyacetylene (TMSA) afforded **4** in 70% yield. Deprotection of the TMS group in **4** with tetrabutylammonium fluoride (TBAF) produced **5** in 82% yield. The cross-coupling reaction of **5** with **Tpd-I** furnished **6** in 63% yield. Subsequent hydrolysis under acidic conditions to strip both the acetyl group and Zn(II) at the same time produced target free-base porphyrin molecule **1** with three mercaptomethyl anchor groups in 84% yield. All new compounds (**1**−**6**) were purified by column chromatography on silica gel and characterized using various spectroscopic methods including ^1H and ^{13}C NMR spectroscopy and ESI- or MALDI-TOF mass spectrometry. More details on the synthesis can be found in the Experimental Section. The thermal analysis data of **1** can be found in the Supporting Information (SI).

The luminescence property of the molecule thus designed and synthesized is our primary concern and needs to be checked before proceeding to the next step. Both steady-state and transient spectral measurements were performed in order to examine the influence of chemical modifications on the optical properties of synthesized molecules. As shown in Figure 2a,b, both the UV−vis absorption and steady-state photoluminescence (PL) spectra of **1** in CH_2Cl_2 solution show characteristic absorption and emission bands similar to those of the tetraphenyl porphyrin moiety,[4,10] also revealing an optical band gap of ∼1.9 eV. In the characteristic double Q-band

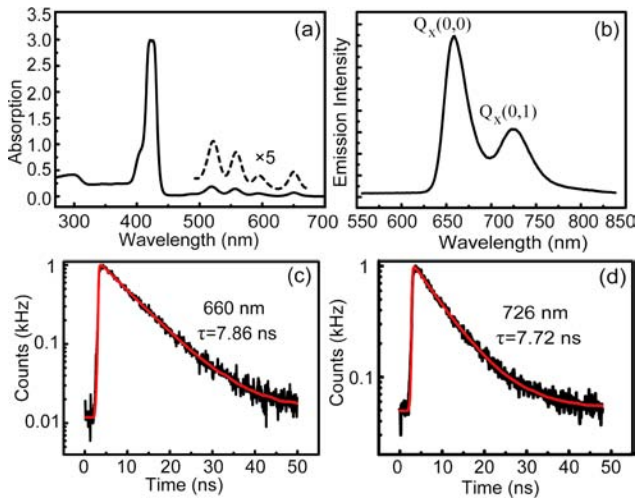

Figure 2. (a) UV−vis absorption and (b) PL spectra of **1** in CH_2Cl_2 solution (∼1.0×10^{-5} mol L^{-1}). The dashed curve in plot a shows magnified data of the Q-band absorption. (c, d) Time-resolved PL decay trace for **1** in CH_2Cl_2 (∼1.0×10^{-8} mol L^{-1}) at 660 and 726 nm, respectively, with pulsed-laser excitation at 405 nm. The black lines are the raw data, and the red lines are the fitting curves.

dx.doi.org/10.1021/ja4048569 | J. Am. Chem. Soc. 2013, 135, 15794−15800

emission associated with the $\pi^*-\pi$ transitions of the conjugate porphyrin plane, the band at ~660 nm is attributed to the $Q_x(0,0)$ transition whereas the band at ~726 nm is attributed to the $Q_x(0,1)$ transition.[4,16] More importantly, the time-resolved fluorescence decay data in Figure 2c,d reveal clear single-exponential decay behavior for both emission bands, with lifetimes of ~7.86 ns at 660 nm and ~7.72 ns at 726 nm. These lifetimes are very close to the monomer lifetime of ~8.38 ns for the tetraphenyl porphyrin,[9] which suggests that the chemical modifications do not generate additional nonradiative channels that would otherwise quench the molecular fluorescence. The designed self-decoupled porphyrin molecule thus appears to be a good candidate as an emitter for STML studies.

For large multifunctionalized molecules such as **1**, vacuum sublimation methods are no longer suitable because the molecules will decompose during heating. Instead, we employed wet-chemistry methods to deposit **1** on Au(111). In an effort to reduce contamination, we first performed the deposition experiment in the load-lock chamber under a nitrogen-gas atmosphere via short-time drop-casting of **1** (~10^{-6} mol/L in CH_2Cl_2) onto the atomically cleaned Au(111) surface.

As shown in Figure 3a, there are isolated multidot features on the STM image of the as-prepared sample, which, for the sake

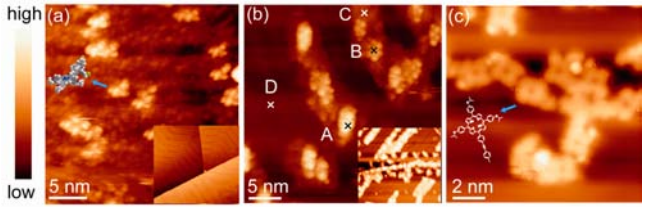

Figure 3. (a) STM image of **1** as prepared via drop-casting on Au(111) (2.8 V, 10 pA, 25 × 25 nm^2). The inset shows the Au(111) surface before deposition (2.5 V, 100 pA, 80 × 80 nm^2). (b) STM image upon annealing at ~310 °C for ~1 h (2.8 V, 20 pA, 30 × 30 nm^2). The inset is an image of a larger area (2.8 V, 5 pA, 75 × 75 nm^2) with a discernible herringbone feature on the bare Au surface. (c) High-resolution image upon further annealing at ~400 °C for ~1 h (2.5 V, 10 pA, 12 × 12 nm^2).

of convenience, could each be visualized as a "dragonfly-like" structure with a length of ~3.3 nm and a width of ~2.5 nm. These dimensions are very close to those estimated for designed self-decoupled porphyrin molecule **1**. Each isolated structure can be approximately considered to consist of four bright dots. The front three-dot pattern may correspond to the three 4-isopropoxyphenyl groups attached to the porphyrin core, whereas the bright dot behind might be assigned to one leg of the tripod with the other two legs bonded to the substrate, as illustrated in the schematic molecular orientation in Figure 3a (more in the SI). All of these topographical features strongly suggest that each isolated dragonfly-like structure corresponds to one target molecule **1**. Nevertheless, its adsorption configuration appears to lie flat on the Au(111) surface rather than standing up with the desired tripod attached to the substrate.[25] The STML measurements on these lying-down molecules exhibit no molecule-specific emission, presumably owing to the quenching of fluorescence originating from insufficient decoupling, misalignment of energy levels at the interface, or the mismatch between the molecular transition dipoles and the axial NCP or a mix of these.

Note that, apart from target molecules **1**, there also exist some unknown impurity molecules (with thiol-related fragments as one possibility) on the surface according to the presence of faint dotlike features between the dragonfly-like structures. To remove these impurities and also to change the adsorption configuration of **1** on Au(111), the sample was annealed at ~310 °C for 1 h. The STM image in Figure 3b shows that the annealing procedure indeed removes most of the impurities and the adsorption configuration of **1** is also changed. The surface appears to be cleaner overall, as illustrated in the inset of Figure 3b (more in Figure S2c of the SI), showing both discernible herringbone structures on the bare Au(111) substrate and a stripelike molecular assembly. However, the higher-resolution image of Figure 3b indicates that the stripelike assembly is composed of a practically two-layer structure with isolated bright units on the top and continuous impurity stripes underneath. These individual bright units on the top, with a feature size of about 3 to 4 nm, are arranged into different packing configurations. Some appear to be single poorly resolved bright protrusions (representative site A), and others form five-dot patterns (representative site B). Although the exact adsorption configurations are unclear, these bright features are believed to associate with the self-decoupled porphyrin molecules of **1**, as confirmed by subsequent annealing and STML studies. As illustrated in Figure 3c, further annealing at a higher temperature of ~400 °C completely removes the impurity molecules from the sample surface. Target molecule **1** is also disassembled, but its porphyrin fragment survives on the surface. The characteristic four-lobed pattern of a tetraphenyl porphyrin unit[10,26] emerges, but with an additional tail that is likely to associate with the (4-methylphenyl)ethynyl group (schematic inset in Figure 3c). In combination with the thermogravimetric analysis data (details in Figure S1 and Scheme S1 in the SI), the tripod appears to break up around this temperature and then desorbs from the surface.

Achieving intrinsic molecular electroluminescence from a single porphyrin molecule is the primary goal in this work. Unlike the absence of molecular fluorescence for flat-lying **1** in the as-prepared sample (Figure 3a), the STML spectrum shown in Figure 4a above site A (Figure 3b) exhibits porphyrin-specific emission of $Q_x(0,0)$ and $Q_x(0,1)$ at ~1.88 and ~1.74

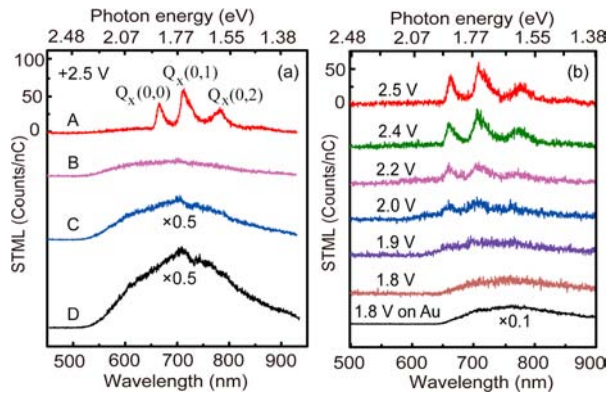

Figure 4. (a) STML spectra on representative sites A–D in Figure 3b (2.5 V, 50 pA, 2 min). (b) Bias dependence of STML spectra on site A (30 pA, 1 min). The STML spectrum on Au(111) is also plotted as a reference (1.8 V, 30 pA, 1 min). The intensities of all STML spectra are normalized by both currents and the acquisition time. Spectra are offset for clarity.

dx.doi.org/10.1021/ja4048569 | J. Am. Chem. Soc. 2013, 135, 15794–15800

eV, respectively. By contrast, the STML spectrum above the porphyrin molecules at site B does not exhibit any molecule-specific fluorescence but only suppressed tip-induced plasmonic emission from the metal substrate.[27−30] The spectral feature is very similar to those acquired on both the impurity layer (site C) and the bare Au surface (site D). The suppression effect of the emission intensity is qualitatively scaled to the topographic height (i.e., the gap distance between the tip and metal substrate).[28,30] The sharp distinction of the STML spectra between sites A and B for target molecule **1** suggests that the molecule at site B still lies flat on the surface, whereas the porphyrin core plane at site A is likely to orient to some extent along the tip axial direction. The latter could provide a considerable vertical component of the transition dipole to couple effectively with the NCP to produce molecular light in the far field. In other words, the molecules at site A are likely either to stand up as designed or to at least be tilted on the substrate, as also supported by the topographic information with the apparent height of site A being higher than that of site B (height profile details in the SI). It is worth pointing out that the additional emission band around 1.59 eV on site A (Figure 4a) can be assigned to the $Q_x(0,2)$ transition. This low-energy emission band is usually invisible in conventional PL measurements and represents one unique characteristic of STM-induced molecular electroluminescence defined by nanoscale plasmonic environments. Its anomalous occurrence suggests the presence of a strong emission enhancement by resonant NCP fields[10] because the tip-induced plasmonic modes on the bare Au (site D in Figure 4a) are very broad, with considerable intensities extending into the low-energy regime. It should be noted that the percentage of fluorescent spots in Figure 3b for the annealed drop-casted sample is very small, less than 5%, and most of them are located at the ends of the bright stripes. For the same tip status, similar spectral shapes could be obtained for similar emitting spots although the intensity might vary.

Further evidence for molecular fluorescence in site A is the nearly constant peak position for each emission band as a function of the excitation voltage (Figure 4b) because the radiative decay of the excited molecule is associated with a given HOMO (the highest-occupied molecular orbital)−LUMO (the lowest-unoccupied molecular orbital) gap. An onset voltage at ∼1.9 V is observed, which is about the same as the optical band gap of the molecule. Above the threshold voltage, the STML intensity rises with increasing bias voltage (up to about 2.8 V) owing to both the growing number of energetically allowed channels that could contribute to photon emission and the enhanced electromagnetic field underneath the tip. Note that the broad emission band at ∼1.8 V in Figure 4b for the site-A molecules originates from the NCP emission alone because its spectral profile is very similar to that acquired on the bare Au surface, though dramatically suppressed as a result of the greatly increased gap distance.

Although molecule-specific emission can be realized on the above drop-casted sample upon annealing, the probability of obtaining molecular electroluminescence is very low and difficult to control. The unfavorable flat-lying adsorption configuration of **1** in the drop-casted sample (Figure 3a) may pertain to the deposition procedure. When the solution is drop-casted on the Au(111) surface under nitrogen flow in the load-lock chamber, the solvent vaporizes too fast to provide sufficient time for all three arms of the tripod to anchor on Au(111) in the liquid state. Therefore, to ensure that molecule **1** has sufficient time to align itself to make better contact with Au(111) in the liquid, we have examined another wet-chemistry method by immersing the Au(111) substrate in the 10^{-6} mol/L CH_2Cl_2 solution of **1** for 10 h at room temperature. (See the SI for more details on the influence of concentration and immersion time on the orientational control of the molecules on Au.)

In contrast to the STM image for the drop-casted sample (Figure 3a), we no longer observe dragonfly-like structures associated with the flat-lying molecules but instead many scattered bright protrusions with a dot dimension in the range of about 3−5 nm (Figure 5a). Although the surface still

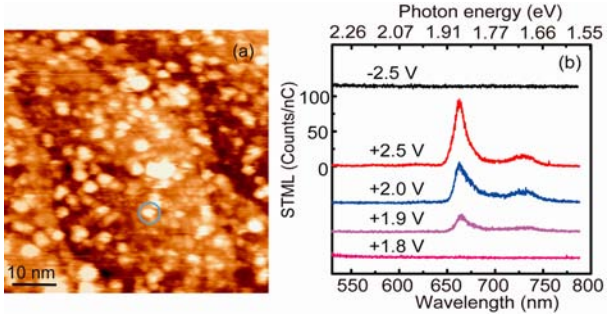

Figure 5. (a) STM image of **1** by immersing Au(111) in the CH_2Cl_2 solution of **1** for 10 h (2.8 V, 10 pA, 60 × 60 nm^2). (b) Bias dependence and polarity dependence of STML spectra on top of the molecules(s) inside the blue circle (50 pA, 1 min). The intensities of all STML spectra are normalized by both the currents and acquisition time. The spectra are offset for clarity.

contains unknown impurity molecules, the step-edge feature of the Au(111) surface is clearly discernible, together with a small portion of bare, exposed Au. All of these observations suggest that the bright protrusion may correspond to either a single molecule of **1** or its aggregate (two to three molecules) standing up directly on the substrate. Such a hypothesis is confirmed by subsequent STML experiments, which indicates that about 60−70% of the bright spots can produce strong molecular electroluminescence. Figure 5b shows the representative STML spectra acquired (e.g., on the dot inside the circle in Figure 5a). Not only is the porphyrin-specific double Q-band emission clearly observed, but also the normalized emission intensity of the strongest peak is larger than that obtained on site A of the annealed drop-casted sample (Figures 3b and 4b). The stronger emission capability for the long-time immersion sample is also supported by the quantum efficiency measurements. A raw photon intensity of ∼460 counts per second (cps) was detected by the single photon avalanched photodiode (SPAD) at 10 pA on the emitting molecules in Figure 5a, which, upon calibration of the photon collection and detection efficiency, gives rise to a quantum efficiency of ∼2 × 10^{-4} photons/electron. Whereas on the emitting molecules at site A for the annealed drop-casted sample in Figure 3b, the quantum efficiency is estimated to be ∼4 × 10^{-5}, about 1 order of magnitude weaker. All of these observations of topographic and spectral features as well as emission intensities suggest that molecule **1** is likely to stand up in the long-time immersion sample, allowing the molecular transition dipole to couple efficiently with the NCP modes to generate strong emission. Note that the low-energy $Q_x(0,2)$ emission at around 1.59 eV in Figure 4 does not show up here because the NCP resonance mode for the tip used for the STML measurements in Figure 5 peaks at around 660 nm, having little plasmonic intensity above

dx.doi.org/10.1021/ja4048569 | J. Am. Chem. Soc. 2013, 135, 15794−15800

750 nm. As a result, the conditions for the emission enhancement of the $Q_x(0,2)$ band cannot be created. These observations demonstrate again the spectral shaping capability of the resonant NCP modes on molecular fluorescence thanks to greatly enhanced radiative decay rates.[10]

Figure 5b also reproduces the onset voltage of molecular electroluminescence at ~1.9 V and increased emission intensity along with the increase in bias voltage. Another important spectral feature in Figure 5b is the highly asymmetric dependency on the bias polarity (e.g., at ±2.5 V). Unlike the ambipolar operation of molecular electroluminescence for multimonolayer molecules,[4,10] the molecule in the present system fluoresces only at positive bias voltages. The origin of such unipolar performance is still not completely clear but is believed to associate with both the energy-level alignment at the molecular interface and the junction asymmetry defined by the tip−molecule−substrate, which could result in different distributions of voltage drops across the STM junction.[31−33] The junction between the tip and molecule is a vacuum barrier, and the contact between the molecule and substrate through the S−Au bonds is quite strong (Figure 6a). Although the

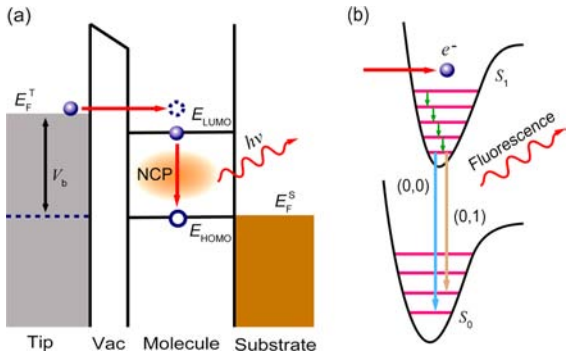

Figure 6. (a) Schematic diagrams showing molecular excitation via hot-electron injection for the positive-sample-bias situation, followed by plasmon-enhanced emission. (b) Molecular fluorescence via a Franck−Condon transition from the excited state (S_1) to the ground state (S_0).

build-in spacer may decouple the interaction of the HOMO and LUMO states of the porphyrin moiety with the substrate to some extent, these frontier molecular orbitals may still be more or less pinned to the substrate and the voltage drop at the molecule−substrate interface could be relatively small. Because the optical band gap of molecule **1** is about 1.9 eV, the occurrence of molecular electroluminescence at positive bias above ~1.9 V suggests that the HOMO level of the molecule under such bias has to align with the Fermi level of the Au substrate so that the HOMO states can be partially emptied to generate holes for radiative combinations with electrons from the LUMO states. However, the absence of molecular electroluminescence at negative bias suggests that in this case it is very difficult, if not impossible, to lift the Fermi surface of the substrate to reach the LUMO level for electron injection within a reasonable bias range that could survive the molecule.

In principle, information about such energy-level alignment could be obtained from the differential conductance (dI/dV) measurements. Nevertheless, because of the relatively "dirty" nature of the wet-chemistry sample preparation method for such a complex multifunctionalized molecule and its relatively large height, it is quite demanding experimentally to obtain well-defined data for topography, $dI/dV-V$ curves, and STML spectra simultaneously using the same tip. Some typical dI/dV data associated with the standing-up molecules are given in the SI, which shows the occurrence of well-defined LUMO states that are peaked at around +2.2(2) V. More importantly, the onset position of the LUMO states in the differential conductance curve appears to correlate approximately with the onset voltage of molecular electroluminescence (more details in the SI).

Furthermore, the unipolar performance also suggests that the NCP field generated by tunneling electrons seems to play a minor role in the excitation of molecules here. Otherwise, because plasmonic excitation is bias-polarity irrelevant, molecular fluorescence should be observed for both polarities. The exact reason for the inefficient excitation of molecules by plasmons in the present system is still unclear but may pertain to the very low efficiency of electron energy being inelastically converted to the NCP emission in the tunneling regime (less than 10^{-3} photons per electron).[27,34−36] As a result, the excitation probability of molecules by plasmons is much smaller compared to the direct excitation via elastic electron injection. However, it should be pointed out that resonant NCP modes are believed to play an important role in the emission enhancement through improving the radiative decay rates.[8,10,14,15] Figure 6 illustrates such an excitation and emission process schematically: when both the HOMO and LUMO levels fall inside the electrochemical potential window defined by the bias voltage, the molecule is excited predominantly by hot electron injection;[4,5] the excited molecule then decays back to the ground state via Franck−Condon $\pi^*-\pi$ transitions with the radiative rate enhanced by the nanocavity plasmons resonant with the selected channels,[10] producing enhanced molecular electroluminescence.

■ CONCLUSIONS

We have successfully designed and synthesized a tripodal porphyrin molecule that could produce molecular electroluminescence on the single-molecule scale. Dipping the Au substrate into the molecular solution for a sufficiently long time is found to be important for the molecule to stand up as desired, with the tripod anchored to the substrate and the porphyrin plane aligned along the tip axial direction. Moreover, the designed self-decoupled molecule makes the tip−molecule−substrate junction highly asymmetric, which enables the observation of a new molecular electroluminescence phenomenon such as the unipolar performance. Our results help us to gain insight into the dominant excitation mechanism via hot-electron injection and emission enhancement through efficient plasmon-exciton coupling. These findings, together with the self-decoupling design to suppress fluorescence quenching, may open up a new way to realize electrically driven single-molecule light sources and to improve the molecule−electrode interface in organic light-emitting diodes.

■ EXPERIMENTAL SECTION

Synthesis of 5-(4-Bromophenyl)-10,15,20-tris-(4-isopropoxyphenyl)porphyrin 2. To a solution containing 4-isopropoxybenzaldehyde (18.71 g, 114 mmol) and 4-bromobenzaldehyde (5.29 g, 28.6 mmol) in 140 mL of propionic acid was added 60 mL of propionic anhydride. After stirring under argon at room temperature for 30 min, the solution was heated to 170 °C and allowed to reflux under the protection of argon with vigorous stirring, and then freshly distilled pyrrole (10 mL, 141 mmol) in propionic acid (10 mL) was added dropwise. After the addition, the reaction mixture was stirred for another 3 h at 170 °C, and then anhydrous ethanol (40

dx.doi.org/10.1021/ja4048569 | J. Am. Chem. Soc. 2013, 135, 15794−15800

mL) was added under vigorous stirring. The mixture was cooled to room temperature and filtered, and the solid product was washed repeatedly with ethanol until the rinsing solution was no longer dark. The filter cake was dissolved in CH_2Cl_2 and chromatographed on silica gel using CH_2Cl_2–petroleum ether (1/1) as the eluent to afford purple crystalline porphyrin **2** (1.51 g, 6%). ^{1}H NMR (400 MHz, $CDCl_3$) δ 8.89 (d, J = 4.8 Hz, 2H), 8.88 (s, 4H), 8.78 (d, J = 4.8 Hz, 2H), 8.09–8.04 (m, 8H), 7.84 (d, J = 8.2 Hz, 2H), 7.23–7.21 (m, 6H), 4.81 (heptet, J = 6.0 Hz, 1H), 4.80 (heptet, J = 6.0 Hz, 2H), 1.53 (d, J = 6.0 Hz, 18H), −2.75 (bs, 2H, NH). ^{13}C NMR (100 MHz, $CDCl_3$) δ 157.9, 141.5, 136.0, 135.8, 134.5, 134.4, 130.0, 122.5, 120.5, 120.3, 118.1, 114.1, 70.3, 22.5. MALDI-TOF-MS m/z: [M$^+$] calcd for $C_{53}H_{47}{}^{79}BrN_4O_3$ 866.2832, found 866.2059.

Synthesis of Zinc(II)-5-(4-bromophenyl)-10,15,20-tris-(4-isopropoxyphenyl)porphyrin 3. A mixture of 5-(4-bromophenyl)-10,15,20-tris-(4-isopropoxyphenyl)porphyrin **2** (1.03 g, 1.19 mmol) and $Zn(OAc)_2{\cdot}2H_2O$ (2.80 g, 12.7 mmol) was dissolved in chloroform–CH_3OH (60 mL, 3/1), and then the mixture was allowed to reflux under argon for 5 h. After the removal of the solvents, the residue was chromatographed on a silica gel column (CH_2Cl_2–petroleum ether, 1/1) to give porphyrin **3** (1.02 g, 93% yield). ^{1}H NMR (400 MHz, $CDCl_3$) δ 8.99–8.96 (m, 6H), 8.86 (d, J = 4.7 Hz, 2H), 8.07–8.02 (m, 8H), 7.81 (d, J = 8.2 Hz, 2H), 7.20–7.16 (m, 6H), 4.77 (heptet, J = 6.0 Hz, 1H), 4.76 (heptet, J = 6.0 Hz, 2H), 1.51 (d, J = 6.0 Hz, 18H). ^{13}C NMR (100 MHz, $CDCl_3$) δ 157.7, 150.9, 150.8, 150.7, 149.9, 142.1, 135.9, 135.6, 135.1, 135.0, 132.4, 132.3, 132.2, 131.5, 129.8, 122.2, 121.5, 121.3, 119.2, 114.0, 70.3, 22.5. MALDI-TOF-MS m/z: [M$^+$] calcd for $C_{53}H_{45}{}^{79}BrN_4O_3Zn$ 928.1967, found 928.0060.

Synthesis of TMS-Protected Zinc(II)-5-(4-ethynylphenyl)-10,15,20-tris-(4-isopropoxyphenyl)porphyrin 4. Air was removed from a single-necked flask containing a mixture of **3** (433.2 mg, 0.47 mmol), $Pd(PPh_3)_2Cl_2$ (84.1 mg, 0.12 mmol), CuI (46.5 mg, 0.24 mmol), and PPh_3 (60.0 mg, 0.23 mmol) in THF–Et_3N (35 mL, 6/1) by argon bubbling for 30 min. Then trimethylsilylacetylene (450 μL, 3.19 mmol) was added, and the mixture was allowed to stir under argon at room temperature for 10 min. Thereafter, the flask was sealed and heated at 80 °C for 48 h. After cooling to room temperature, the solvent was evaporated, and the crude product was purified on a silica gel column (CH_2Cl_2–petroleum ether, 1/1) to provide TMS-protected porphyrin **4** (308.5 mg, 70% yield). ^{1}H NMR (400 MHz, $CDCl_3$) δ 8.97 (d, J = 4.7 Hz, 2H), 8.96 (s, 4H), 8.86 (d, J = 4.7 Hz, 2H), 8.12 (d, J = 8.2 Hz, 2H), 8.054 (d, J = 8.6 Hz, 2H), 8.047 (d, J = 8.6 Hz, 4H), 7.85 (d, J = 8.2 Hz, 2H), 7.23 (d, J = 8.6 Hz, 6H), 4.84 (heptet, J = 6.0 Hz, 3H), 1.56 (d, J = 6.0 Hz, 18H), 0.38 (s, 9H). ^{13}C NMR (100 MHz, $CDCl_3$) δ 157.8, 150.8, 150.73, 150.68, 149.9, 143.5, 135.6, 135.11, 135.07, 134.5, 132.4, 132.2, 132.1, 131.6, 130.4, 122.4, 121.4, 121.2, 119.9, 114.0, 105.4, 95.4, 70.3, 22.5, 0.3. MALDI-TOF-MS m/z: [M$^+$] calcd for $C_{58}H_{54}N_4O_3SiZn$ 946.3257, found 946.2683.

Synthesis of Zinc(II)-5-(4-ethynylphenyl)-10,15,20-tris-(4-isopropoxyphenyl)porphyrin 5. Porphyrin **4** (308.5 mg, 0.33 mmol) was dissolved in distilled THF (30 mL) and stirred under an argon atmosphere for 15 min. Then tetrabutylammonium fluoride (1.69 g, 6.48 mmol) was added. The mixture was stirred under argon for 1 h and then diluted with dichloromethane (100 mL) and washed twice with water. The organic phase was collected and dried over anhydrous sodium sulfate. The solvent was removed under reduced pressure, and the crude product was purified on a silica gel column (CH_2Cl_2–petroleum ether, 1/1) to yield porphyrin **5** (235.0 mg, 82% yield). ^{1}H NMR (400 MHz, $CDCl_3$) δ 9.00 (d, J = 4.7 Hz, 2H), 8.99 (s, 4H), 8.90 (d, J = 4.7 Hz, 2H), 8.18 (d, J = 8.2 Hz, 2H), 8.10 (d, J = 8.5 Hz, 2H), 8.09 (d, J = 8.5 Hz, 4H), 7.88 (d, J = 8.2 Hz, 2H), 7.25 (d, J = 8.4 Hz, 6H), 4.86 (heptet, J = 6.0 Hz, 3H), 3.30 (s, 1H), 1.57 (d, J = 6.0 Hz, 18H). ^{13}C NMR (100 MHz, $CDCl_3$) δ 157.8, 150.9, 150.74, 150.68, 149.9, 143.8, 135.6, 135.1, 135.0, 134.5, 132.4, 132.24, 132.16, 131.6, 130.5, 121.5, 121.4, 121.3, 119.8, 114.0, 84.0, 78.2, 70.3, 22.5. MALDI-TOF-MS m/z: [M$^+$] calcd for $C_{55}H_{46}N_4O_3Zn$ 874.2861, found 874.2104.

Synthesis of Porphyrin 6. A solution of porphyrin **5** (219.8 mg, 0.25 mmol) and 1-(4-iodophenyl)-1,1,1-tris[4-(*S*-acetylthiomethyl)-phenyl]methane (268.7 mg, 0.38 mmol) in dry toluene–triethylamine (18 mL, 5/1) was purged with argon for 30 min. The coupling was initiated by adding PPh_3 (113.0 mg, 0.43 mmol) followed by $Pd_2(dba)_3$ (114.5 mg, 0.13 mmol), and the reaction mixture was then stirred at 30 °C for 7 days until thin-layer chromatography (TLC) monitoring indicated the formation of new spots and the disappearance of **5**. The crude reaction mixture was purified by silica gel chromatography using petroleum ether/dichloromethane (1/2) as the eluent to furnish porphyrin **6** (230.7 mg, 63% yield). ^{1}H NMR (400 MHz, $CDCl_3$) δ 8.99 (d, J = 4.6 Hz, 2H), 8.98 (s, 4H), 8.92 (d, J = 4.6 Hz, 2H), 8.18 (d, J = 8.1 Hz, 2H), 8.08 (d, J = 8.4 Hz, 6H), 7.88 (d, J = 8.1 Hz, 2H), 7.54 (d, J = 8.5 Hz, 2H), 7.24–7.21 (m, 6H), 7.15–7.03 (m, 14H), 4.88–4.79 (m, 3H), 3.96 (s, 6H), 2.21 (s, 9H), 1.55 (d, J = 6.0 Hz, 18H). ^{13}C NMR (100 MHz, $CDCl_3$) δ 195.3 (C=O), 157.7, 150.8, 150.7, 150.6, 149.9, 147.1, 145.4, 143.3, 143.2, 135.6, 135.4, 135.13, 135.10, 134.6, 132.3, 132.2, 132.1, 131.6, 131.3, 131.2, 131.1, 130.0, 129.0, 128.9, 128.4, 128.2, 127.4, 122.5, 121.3, 121.1, 119.9, 114.0, 90.3, 89.8, 70.3, 64.4, 33.0, 30.3, 22.5. MALDI-TOF-MS m/z: [M$^+$] calcd for $C_{89}H_{76}N_4O_6S_3Zn$ 1456.4218, found 1456.4545.

Synthesis of Porphyrin 1. Porphyrin **6** (43.2 mg, 0.03 mmol) was placed in a 250 mL three-necked round-bottomed flask and dissolved with degassed CH_2Cl_2 (56 mL) and degassed MeOH (28 mL). Concentrated H_2SO_4 (5.6 mL) was added dropwise to the mixture at 0 °C. The mixture was then gradually warmed to 60 °C with stirring. After stirring for 12 h, the reaction was quenched by the addition of water, and the organic layer was separated. The aqueous layer was extracted with CH_2Cl_2, and the combined organic layer was washed with brine and dried over Na_2SO_4. After the removal of the solvent under reduced pressure, the residue was purified by column chromatography on silica gel with CH_2Cl_2 as the eluent to give target molecule **1** (31.6 mg, 84% yield). ^{1}H NMR (400 MHz, $CDCl_3$) δ 8.90 (d, J = 4.8 Hz, 2H), 8.89 (s, 4H), 8.83 (d, J = 4.8 Hz, 2H), 8.19 (d, J = 8.1 Hz, 2H), 8.09 (d, J = 8.4, 6H), 7.89 (d, J = 8.0 Hz, 2H), 7.56 (d, J = 8.4 Hz, 2H), 7.29–7.19 (m, 20H), 4.85 (heptet, J = 6.1 Hz, 3H), 3.74 (d, J = 7.5 Hz, 6H), 1.79 (t, J = 7.5 Hz, 3H), 1.56 (d, J = 6.1 Hz, 18H), −2.74 (bs, 2H, NH). ^{13}C NMR (100 MHz, $CDCl_3$) δ 157.9, 147.3, 145.33, 145.27, 142.6, 139.0, 135.9, 134.8, 134.5, 134.4, 131.4, 131.23, 131.18, 130.1, 127.5, 122.8, 121.1, 120.5, 120.2, 118.9, 114.1, 90.5, 89.8, 70.3, 64.5, 28.6, 22.5. ESI-MS m/z: [M + H$^+$] calcd for $C_{83}H_{72}N_4O_3S_3$ 1268.4767, found 1269.4840.

Theoretical Calculation. The geometry of **1** was calculated at the B3LYP/6-31G(d) level with Gaussian 09W without a consideration of the effect of the substrate.

Acquisition of Photoluminescence Spectra and Measurement of Photoluminescence Lifetimes. The acquisition of PL spectra and the measurement of fluorescence lifetimes were carried out on a home-built optical setup. Steady-state spectra were recorded with a liquid-nitrogen-cooled charge-coupled-device (CCD) spectrometer (Princeton Instruments) under the excitation of light at 405 nm. The time-correlated single-photon counting technique (Edinburgh Instruments) was used to determine the fluorescence lifetimes. The time resolution was ~8 ps with the use of a microchannel plate photomultiplier tube and a pulse picosecond diode laser at 405 nm (Hamamatsu). A cutoff filter at 470 nm was used to block the excitation light. The time-resolved PL curves were fitted with an exponential function.

Molecular Deposition on Au(111). After being synthesized and purified, molecule **1** was immediately dissolved in CH_2Cl_2 at a concentration of ~1.0×10^{-6} M.

Wet-Chemistry Method via Short-Time Drop-Casting. The drop-casted sample was prepared by dripping 10 μL of a solution of **1** onto the atomically cleaned Au(111) surface in the load-lock chamber under a nitrogen-gas atmosphere. The solvent evaporated within seconds, and the chamber was immediately pumped under vacuum. The sample was then transferred to the ultrahigh-vacuum (UHV) observation chamber for STM investigations at low temperature (~80 K).

Wet-Chemistry Method via Long-Time Immersion. The freshly prepared Au(111) substrate was immersed in the solution for 10 h at room temperature. Then the substrate was removed from the solution,

dx.doi.org/10.1021/ja4048569 | J. Am. Chem. Soc. 2013, 135, 15794–15800

rinsed thoroughly with CH_2Cl_2 10 times, and dried under a stream of nitrogen gas before being loaded into the UHV chamber for STM investigations at low temperature (~80 K). The influence of concentration and immersion time on the adsorption configuration of the target molecule on Au is briefly described in the SI.

Scanning Tunneling Microscope-Induced Luminescence. The experiments were performed with a low-temperature UHV-STM (Unisoku) at a base pressure of ~8×10^{-11} mbar at ~80 K, operated in the constant-current−topographic mode with the sample biased. The Au(111) substrate was prepared by the thermal evaporation of gold (~150 nm thick) on freshly cleaved mica and cleaned in UHV by cycles of argon ion sputtering. Electrochemically etched silver (Ag) tips were used to perform STM imaging and STML measurements, taking advantage of silver in producing strong plasmonic fields.[35]

Photons emitted from the tunnel junction were collected with a lens inside the UHV chamber and then refocused into an optical fiber by another lens placed outside the UHV chamber. The collected light was guided into a grating spectrometer and analyzed by a cooled CCD detector (Princeton Instruments) for spectral information.[10,35,36] Photon intensities, measured by the SPAD (PerkinElmer, ~72% detection efficiency of around 660 nm), were corrected for the detection efficiency of the SPAD and the collection efficiency of both the lens system (~10%) and the beamsplitter (50%).[36] Nevertheless, luminescence spectra presented in the article were not corrected for the wavelength-dependent sensitivity of photon collection and detection systems.

■ ASSOCIATED CONTENT

Supporting Information

Experimental procedures for the synthesis of **Tpd-I**, thermogravimetric analysis, additional STM and tunneling spectral information, Cartesian coordinates of molecule **1**, and NMR spectra of synthesized compounds. This material is available free of charge via the Internet at http://pubs.acs.org.

■ AUTHOR INFORMATION

Corresponding Authors

gwang@ustc.edu.cn
zcdong@ustc.edu.cn

Author Contributions

S.-E.Z. and Y.-M.K. contributed equally.

Notes

The authors declare no competing financial interest.

■ ACKNOWLEDGMENTS

We thank Andre Gourdon for helpful discussions on the molecular design. This work is supported by NBRPC (2011CB921402), CAS (XDB01020000), and NSFC (91021004 and 10974186).

■ REFERENCES

(1) Coombs, J. H.; Gimzewski, J. K.; Reihl, B.; Sass, J. K.; Schlittler, R. R. *J. Microsc.* **1988**, *152*, 325.
(2) Berndt, R.; Gaisch, R.; Gimzewski, J. K.; Reihl, B.; Schlittler, R. R.; Schneider, W. D.; Tschudy, M. *Science* **1993**, *262*, 1425.
(3) Qiu, X. H.; Nazin, G. V.; Ho, W. *Science* **2003**, *299*, 542.
(4) Dong, Z. C.; Guo, X. L.; Trifonov, A. S.; Dorozhkin, P. S.; Miki, K.; Kimura, K.; Yokoyama, S.; Mashiko, S. *Phys. Rev. Lett.* **2004**, *92*, 086801.
(5) Ćavar, E.; Blüm, M.-C.; Pivetta, M.; Patthey, F.; Chergui, M.; Schneider, W.-D. *Phys. Rev. Lett.* **2005**, *95*, 196102.
(6) Chance, R. R.; Prock, A.; Silbey, R. *Adv. Chem. Phys.* **1978**, *37*, 1.
(7) Barnes, W. L. *J. Mod. Opt.* **1998**, *45*, 661.
(8) Anger, P.; Bharadwaj, P.; Novotny, L. *Phys. Rev. Lett.* **2006**, *96*, 113002.
(9) Zhang, X.-L.; Chen, L.-G.; Lv, P.; Gao, H.-Y.; Wei, S.-J.; Dong, Z.-C.; Hou, J. G. *Appl. Phys. Lett.* **2008**, *92*, 223118.
(10) Dong, Z. C.; Zhang, X. L.; Gao, H. Y.; Luo, Y.; Zhang, C.; Chen, L. G.; Zhang, R.; Tao, X.; Zhang, Y.; Yang, J. L.; Hou, J. G. *Nat. Photonics* **2010**, *4*, 50.
(11) Kabakchiev, A.; Kuhnke, K.; Lutz, T.; Kern, K. *Chem. Phys. Chem.* **2010**, *11*, 3412.
(12) Matino, F.; Schull, G.; Köhler, F.; Gabutti, S.; Mayor, M.; Berndt, R. *Proc. Natl. Acad. Sci. U.S.A.* **2011**, *108*, 961.
(13) Schneider, N. L.; Matino, F.; Schull, G.; Gabutti, S.; Mayor, M.; Berndt, R. *Phys. Rev. B* **2011**, *84*, 153403.
(14) Mills, D. L. *Phys. Rev. B* **2002**, *65*, 125419.
(15) Kühn, S.; Mori, G.; Agio, M.; Sandoghdar, V. *Mol. Phys.* **2008**, *106*, 893.
(16) Milgrom, L. R. *The Colour of Life: An Introduction to the Chemistry of Porphyrin and Related Compounds*; Oxford University Press: New York, 1997.
(17) Davis, G. L.; Hey, D. Y.; Williams, G. H. *J. Chem. Soc.* **1956**, 4397.
(18) Heim, C.; Affeld, A.; Nieger, M.; Vögtle, F. *Helv. Chim. Acta* **1999**, *82*, 746.
(19) Zhu, L.; Tang, H.; Harima, Y.; Yamashita, K.; Hirayama, D.; Aso, Y.; Otsubo, T. *Chem. Commun.* **2001**, 1830.
(20) Hirayama, D.; Takimiya, K.; Aso, Y.; Otsubo, T.; Hasobe, T.; Yamada, H.; Imahori, H.; Fukuzumi, S.; Sakata, Y. *J. Am. Chem. Soc.* **2002**, *124*, 532.
(21) Wei, L.; Padmaja, K.; Youngblood, W. J.; Lysenko, A. B.; Lindsey, J. S.; Bocian, D. F. *J. Org. Chem.* **2004**, *69*, 1461.
(22) Sakata, T.; Maruyama, S.; Ueda, A.; Otsuka, H.; Miyahara, Y. *Langmuir* **2007**, *23*, 2269.
(23) Ie, Y.; Hirose, T.; Yao, A.; Yamada, T.; Takagi, N.; Kawai, M.; Aso, Y. *Phys. Chem. Chem. Phys.* **2009**, *11*, 4949.
(24) Adler, A. D.; Longo, F. R.; Finarelli, J. D.; Goldmacher, J.; Assour, J.; Korsakoff, L. *J. Org. Chem.* **1967**, *32*, 476.
(25) Schramm, A.; Stroh, C.; Dössel, K.; Lukas, M.; Fischer, M.; Schramm, F.; Fuhr, O.; v. Löhneysen, H.; Mayor, M. *Eur. J. Inorg. Chem.* **2013**, *2013*, 70.
(26) Jung, T. A.; Schlittler, R. R.; Gimzewski, J. K. *Nature* **1997**, *386*, 696.
(27) Berndt, R.; Gimzewski, J. K.; Johansson, P. *Phys. Rev. Lett.* **1991**, *67*, 3796.
(28) Tao, X.; Dong, Z. C.; Yang, J. L.; Luo, Y.; Hou, J. G.; Aizpurua, J. *J. Chem. Phys.* **2009**, *130*, 084706.
(29) Zhang, Y.; Geng, F.; Gao, H. Y.; Liao, Y.; Dong, Z. C.; Hou, J. G. *Appl. Phys. Lett.* **2010**, *97*, 243101.
(30) Geng, F.; Zhang, Y.; Yu, Y.; Kuang, Y.; Liao, Y.; Dong, Z.; Hou, J. *Opt. Express* **2012**, *20*, 26725.
(31) Zahid, F.; Paulsson, M.; Datta, S. Electrical Conduction through Molecules. In *Advanced Semiconductors and Organic Nano-Techniques*; Morkoc, H., Ed.; Academic Press: New York, 2003; Vol. *III*, pp 1−41.
(32) Wu, S. W.; Nazin, G. V.; Chen, X.; Qiu, H. X.; Ho, W. *Phys. Rev. Lett.* **2004**, *93*, 236802.
(33) Niquet, Y. M.; Delerue, C.; Allan, G. *Phys. Rev. B* **2002**, *65*, 165334.
(34) Johansson, P. *Phys. Rev. B* **1998**, *58*, 10823.
(35) Zhang, C.; Gao, B.; Chen, L. G.; Meng, Q. S.; Yang, H.; Zhang, R.; Tao, X.; Gao, H. Y.; Liao, Y.; Dong, Z. C. *Rev. Sci. Instrum.* **2011**, *82*, 083101.
(36) Chen, L. G.; Zhang, C.; Zhang, R.; Zhang, X. L.; Dong, Z. C. *Rev. Sci. Instrum.* **2013**, *84*, 066106.